Soil Dynamics and Earthquake Engineering 30 (2010) 1182–1197

Contents lists available at ScienceDirect

Soil Dynamics and Earthquake Engineering

journal homepage: www.elsevier.com/locate/soildyn

# Interstory drift ratio of building structures subjected to near-fault ground motions based on generalized drift spectral analysis

Dixiong Yang, Jianwei Pan, Gang Li *

*Department of Engineering Mechanics, State Key Laboratory of Structural Analysis for Industrial Equipment, Dalian University of Technology, Dalian 116024, China*

ARTICLE INFO

*Article history:*
Received 24 January 2009
Received in revised form
22 April 2010
Accepted 27 April 2010

ABSTRACT

This paper focuses on the interstory drift ratio (IDR) demands of building structures subjected to near-fault ground motions having different impulsive characteristics based on generalized interstory drift spectral analysis. The near-fault ground motions considered include the idealized simple pulses and three groups of near-fault ground motions with forward directivity pulses, fling-step pulses and without velocity pulse. Meanwhile, the building systems are equivalently taken as shear-flexural beams with representative lateral stiffness ratios. The IDR distribution of continuous beams subjected to three groups of near-fault ground motions is acquired. It is illustrated that the maximum IDR shifts from the upper half to the lower half of buildings with an increase in lateral stiffness ratio. For long-period systems, the average IDR under impulsive ground motions is significantly greater than that under non-pulse motions. Finally, for moment-resisting frame buildings the forward directivity pulses amplify the drift response of higher modes, while the fling-step pulses excite primarily their contribution in the first mode and generate large deformation in the lower stories. The essential reason for this phenomenon is revealed according to the distinct property of near-fault impulsive ground motions and generalized drift spectral analysis.

© 2010 Elsevier Ltd. All rights reserved.

## 1. Introduction

Interstory drift ratio (IDR) is an important damage demand parameter of building structures under earthquake loads. Consequently, the correct and convenient evaluation on maximum interstory drift is fairly significant to seismic analysis and design of buildings. Based on the continuous shear-beam model and wave propagation theory, Iwan [1] proposed an interstory drift spectral method to directly compute the interstory deformation under earthquake action, especially near-fault ground motions with long-period pulses. Despite its new concept and its many characteristics superior to traditional response spectrum, the early drift spectrum has some limitations. For instance, Chopra and Chintanapakdee [2] showed that the wave propagation analysis cannot be well grasped by structural engineers and the drift spectrum can also be calculated using modal analysis techniques. Kim and Collins [3] pointed out that the original formulation of drift spectrum corresponds to a cantilever shear-beam model attached to external springs with dampers anchored to a fixed point, and this formula results in residual drifts for certain ground motions.

Later, some improvements about the drift spectrum are carried out [4–11]. Sanani et al. [9] improved the wave propagation model of shear beam to properly account for the dispersive type of damping. Zembaty [10] implemented a random vibration analysis of shear beam under non-stationary excitations in terms of modal superposition. These works are all based on the pure shear-beam model, which cannot characterize the flexural structures. However, it is worth noting that Miranda and Akkar [11] developed the generalized interstory drift spectrum according to a versatile shear-flexural beam model and modal superposition technique, so that it can estimate rapidly the elastic interstory drift demands and acceleration and force responses of high-rise buildings with different lateral stiffness ratios representing various kinds of structures.

Near-fault ground motions are generally referred to as the ground motions of site within a distance of about 20 km from the rupture fault, which is significantly different from those at far-fault region. The distinct characteristics of near-fault ground motions are originated from the rupture forward directivity, fling-step effect, hanging wall effect, etc [12–17]. Due to the former two effects, the near-fault ground motions usually show two important characteristics: a pulse-like velocity waveform and a permanent ground displacement, which had caused severe structural damage in recent major earthquakes, e.g., Northridge in 1994, Kobe in 1995 and Chi-Chi, Taiwan in 1999 and Wen-Chuan, China in 2008, etc. Especially in recent years, the

* Corresponding author, Tel.: +86 411 84707267, fax: +86 411 84707267.
*E-mail addresses:* yangdx@dlut.edu.cn (D. Yang), gege_607@163.com (J. Pan), ligang@dlut.edu.cn (G. Li).

0267-7261/$ - see front matter © 2010 Elsevier Ltd. All rights reserved.
doi:10.1016/j.soildyn.2010.04.026

characteristics of near-fault ground motions and their effect on engineering structures are very important research topics to both the seismological and engineering communities [18–29].

The rupture forward directivity occurs when a fault rupture propagates towards a site with a rupture velocity close to the shear-wave velocity [12–13,15–17,27]. The forward directivity conditions can be present for both strike-slip fault and dip-slip events. This phenomenon causes most of the seismic energy from the rupture process to arrive in a single large, long-period pulse at the beginning of the record in a short duration. The intense velocity pulse is primarily oriented in the fault-normal direction because of the radiation pattern of the shear dislocation on the fault plane.

On the other hand, pulse-like motions can be also generated by fling step, i.e. the permanent ground displacements associated with surface rupture and tectonic deformation. The characteristic of pulses from the fling step differs from that of the rupture forward directivity. Generically, fling step is the result of a permanent ground displacement that generates one-sided velocity pulses, whereas forward directivity is a dynamic phenomenon that produces no permanent ground displacement and hence two-sided (reversing) velocity pulses [12,16–17,19,27]. It is believed that the reversing pulse motion in a fault-normal component is potentially more damaging than the one-sided pulse [19,27]. Fling step is observed as a distinct step in a displacement time history in the fault-parallel direction for strike-slip earthquakes or in the fault-normal direction for dip-slip events [12,16–17,27]. For strike-slip events, the forward directivity pulses are partitioned mainly in the strike-normal direction, whereas the fling-step effects are partitioned in the fault-parallel direction. If the static ground displacement is removed from the fault-parallel component, very little dynamic motion remains. For dip-slip events, the forward directivity and the fling-step effects are both coupled to the fault-normal component, and there is a little of either motions on the strike-parallel component [12,16–17]. If the static ground displacement is removed from the fault-normal component, a large forward directivity pulse remains.

As is known, the near-fault pulse-like ground motions transmit high energy to the structure at the onset of earthquake, thus resulting in an intensive structural damage. Accordingly, many efforts are made to examine the seismic response of engineering structures subjected to forward directivity pulses of ground motions [18–27,30–31]. For example, Krawinkler et al. [30] and Alavi and Krawinkler [24,31] analyzed the seismic drift and ductility demands of moment-resisting frame structures under near-fault ground motions with forward directivity pulses. Unfortunately, a few investigations account for different effects between fling-step pulses and forward directivity pulses of near-fault ground motions on structural responses, except the recent work of Kalkan and Kunnath [17]. They evaluated the influence of two kinds of velocity pulses of near-fault records on the inelastic seismic demands of three steel-frame buildings with 4, 6 and 13 stories, respectively. It was demonstrated that although the fling effects on buildings are less significant than the forward directivity in the upper and intermediate levels, the systems subjected to records with fling-step pulses respond primarily to the lower stories. But they did not explain theoretically the reason why this phenomenon occurs based on the distinct characteristic of impulsive ground motions.

Actually, the influences of near-fault ground motions with different impulsive characteristics on structural seismic responses should be scrutinized carefully for seismic design and safety assessment of engineering structures. This paper aims to investigate different effects of the two types of velocity pulses of near-fault ground motions with forward directivity and fling step on the IDR of buildings, from the perspective of theory and computation, using the generalized interstory drift spectrum. Three sets of near-fault ground motions are assembled containing forward directivity pulses, fling-step pulses and non-pulse motions, respectively. Furthermore, the idealized simple pulses are introduced to simulate the impulsive near-fault ground excitations. Meanwhile, the building systems are equivalently taken as shear-flexural beams with representative lateral stiffness ratios and representative fundamental periods (i.e. $T_1=0.3$, 1.0 and 3.0 s corresponding to stiff building, intermediate-period and flexible building systems, respectively). According to the generalized drift spectral analysis, the IDR distribution of various types of building structures over the height are obtained and compared. Moreover, the essential reason for the IDR distribution mode of moment-resisting frame buildings subjected to near-fault ground motions is revealed, which is another key objective of this work.

## 2. Generalized interstory drift spectrum of shear-flexural beam

The interstory drift ratio of building structures is one of the most important damage parameters corresponding to damage potential of strong earthquake ground motions. Based on interstory drift spectrum earlier proposed by Iwan [1], the generalized drift spectrum of a shear-flexural beam is extended by Miranda and Akkar [11] to quickly estimate the IDR and force responses of high-rise buildings under ground motions, insensitive to the variation of lateral stiffness [32]. The dynamic response of undamped uniform shear-flexural beam shown in Fig. 1 under a horizontal acceleration $\ddot{u}_g(t)$ at the base is expressed as a partial differential equation [11]

$$\frac{\rho}{EI}\frac{\partial^2 u(x,t)}{\partial t^2}+\frac{1}{H^2}\frac{\partial^4 u(x,t)}{\partial t^4}-\frac{\alpha^2}{H^4}\frac{\partial^2 u(x,t)}{\partial x^2}=-\frac{\rho}{EI}\frac{\partial^2 u_g(t)}{\partial t^2} \tag{1}$$

where $\rho$ denotes the mass per unit length in the model; $H$ is the total height of the building; $u(x,t)$ represents the lateral displacement at the dimensionless height $x=z/H$, which varies between zero at the base of the building and one at the roof level at time $t$; $EI$ means the flexural stiffness of the flexural beam and $\alpha$ is the lateral stiffness ratio written as

$$\alpha=H\sqrt{\frac{GA}{EI}} \tag{2}$$

where $GA$ denotes shear stiffness of the shear beam. A value of $\alpha$ equal to zero corresponds to a pure flexural beam and $\alpha$ equal to

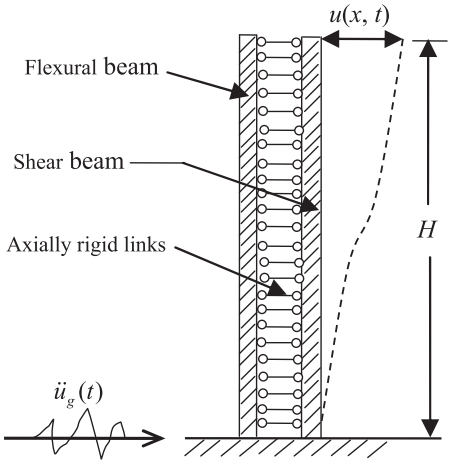


**Fig. 1.** Continuous beam model in generalized interstory drift spectrum.

infinity represents a pure shear-beam model. The lateral deflected shapes of buildings whose lateral resisting system consists only of structural walls can usually be approximated by using the values of $\alpha$ between 0 and 2. Moreover, for buildings with dual lateral resisting systems consisting of a combination of moment-resisting frames and shear walls or a combination of moment-resisting frames and braced frames, the values of $\alpha$ are commonly between 1.5 and 6, while for buildings whose lateral resisting system consists only of moment-resisting frames the values of $\alpha$ are typically between 5 and 20 [11,32].

The total displacement response of the system can be computed by modal superposition as

$$u(x,t) = \sum_{i=1}^{\infty} u_i(x,t) \tag{3}$$

Assuming that the system is classically damped, the contribution of the $i$th mode of vibration to the lateral displacement at relative height $x=z/H$ at time $t$ is shown as

$$u_i(x,t) = \Gamma_i \phi_i D_i(t) \tag{4}$$

where $\Gamma_i$ is the modal participation factor of the $i$th mode of vibration; $\phi_i$ denotes the amplitude of the $i$th mode at non-dimensional height $x$; $D_i(t)$ represents the relative displacement response of a single degree of freedom (SDOF) elastic system with the period of the $i$th mode $T_i$ and modal damping ratio $\xi_i$ subjected to a given ground acceleration $\ddot{u}_g(t)$.

The derivative of lateral displacement in Eq.(3) with respect to $x$ provides the rotation response history at dimensionless height $x$

$$\theta(x,t) = \frac{\partial u(x,t)}{\partial x} = \frac{1}{H}\sum_{i=1}^{\infty} \Gamma_i \phi_i'(x) D_i(t) \tag{5}$$

where $\phi_i'(x)$ represents the first derivative of the $i$th mode shape $\phi_i(x)$ with respect to dimensionless height $x$.

The IDR of buildings is defined as the difference of displacements at the adjacent two floors normalized by the interstory height. Here, the IDR at the $j$th story is approximated by the rotation in the beam model at the height corresponding to the middle of the story of interest as follows [11]:

$$\mathrm{IDR}(j,t) \approx \theta(x,t) = \frac{1}{H}\sum_{i=1}^{\infty} \Gamma_i \phi_i'(x) D_i(t) \tag{6}$$

where $x$ is the average height of the $j+1$ and $j$ floors.

Actually, for Eq.(6) in most cases only a relatively small number of modes is sufficient to obtain good estimates of the peak rotation demand in the beam model [1,11]. Hence, the IDR at dimensionless height $x$ can be approximated as

$$\mathrm{IDR}(x,t) \approx \frac{1}{H}\sum_{i=1}^{m} \Gamma_i \phi_i'(x) D_i(t) \tag{7}$$

where $m$ denotes the number of vibration modes considered in the spectral analysis.

The generalized interstory drift spectrum is a plot of the fundamental period $T$ of the building versus the maximum IDR. The ordinates of a generalized drift spectrum are defined as the maximum peak rotation over the height of the building and IDR is computed as

$$\mathrm{IDR} = \max_{\forall x,t} |\theta(x,t)| \approx \max_{\forall x,t} \left| \frac{1}{H}\sum_{i=1}^{m} \Gamma_i \phi_i'(x) D_i(t) \right| \tag{8}$$

Finally, it should be pointed out that the main assumption behind the applied modal superposition technique in generalized interstory drift spectrum is that the modal responses are assumed to be uncoupled, which is not the case for a structural system when its response extends into a nonlinear range. In nonlinear domain, the modal shapes and corresponding modal participation factors may be significantly altered owing to the reduction of stiffness in building system.

## 3. Data of near-fault ground motions with forward directivity and fling-step effects

The data of near-fault ground motion records with forward directivity and fling-step effects are selected from the Northridge earthquake (1994, 1, 17, $M_W$=6.7) and Chi-Chi earthquake (1999, 9, 21, $M_W$=7.6). It should be noted that some procedures of data processing can filter and remove the permanent displacement of raw ground motions containing fling-step effect [17,27,28]. Herein, the near-fault records of Chi-Chi earthquake are chosen from the database processed by Wang et al. [14], which reserved well the fling-step effect. The near-fault ground motion records of Northridge earthquake are taken from the strong motion database in Pacific Earthquake Engineering Research Center. Because the records with fling-step pulses in the existing database are quite limited, ten different records having the character of fling step and forward directivity are used here. Table 1 lists the important parameters of three groups of near-fault ground motions such as the closet distance to fault rupture $d$, site condition $S$, $PGA$ (peak ground acceleration), $PGV$, $PGD$, $PGV/PGA$, predominant period of pulse $T_{PV}$ (which corresponds to the period where the pseudo spectral velocity reaches its maximum, and is used to characterize the pulse period $T_P$ because it is correlated well with the latter [26–28]) and 95% significant duration $t_d$ [29]. The closet distance to rupture these records is smaller than 20 km, whereas $PGA$ is larger than 0.1 g and $PGV$ is greater than 30 cm/s. In order to avoid the interference to the nature of near-fault ground motions, these original records are employed and no scaling is performed in the generalized drift spectral analysis in the next sections.

The velocity pulses of near-fault ground motions with forward directivity or fling-step effects in Table 1 depend on their waveforms of velocity and displacement time histories. Generally speaking, the large ratios of $PGV/PGA$ of ground motions imply that these records could contain velocity pulses, and for the non-pulse ground motions the ratios of $PGV/PGA$ are usually smaller than 0.20 [22]. Furthermore, the impulsive ground motions have larger predominant periods $T_{PV}$, while the non-pulse ground motions have smaller predominant periods. Fig. 2 shows the velocity and displacement time histories of near-fault ground motion RRS-228 with forward directivity pulse where its velocity pulse displays two-sided (reversing) form. Fig. 3 illustrates the velocity and displacement time histories of near-fault ground motion TCU052-NS with fling-step pulse where its velocity pulse displays one-sided (non-reversing) form, and the displacement time history exhibits the distinctive large step corresponding to the permanent ground displacement.

## 4. Simple pulses and their generalized drift spectra

The structural effects of near-fault ground motions are associated with the impulsive nature of these ground excitations. Accordingly, there are a substantial number of simplified pulse representations that attempt to capture the salient features of near-fault ground motions within limitations [17,19,21,23–25,28,33]. Many acceleration formulations of pulse are simply square, triangular or trigonometric functions, but some representations are more complicated [23,25]. However, it is unreasonable to expect that the simple pulses can represent accurately and fully the impulsive waveforms of near-fault ground motions. Despite the limitations of simple pulses, it is

**Table 1**
Basic parameters of three groups of near-fault ground motions.

| Ground motions | Station, component | $d$ (km) | $S$ | $PGA$ (g) | $PGV$ (cm/s) | $PGD$ (cm) | $PGV/PGA$ (s) | $T_{PV}$ (s) | $t_d$ (s) |
|---|---|---|---|---|---|---|---|---|---|
| Forward directivity pulse | TCU051-EW | 6.95 | C | 0.160 | 51.53 | 124.52 | 0.27 | 6.6 | 24.18 |
| | TCU054-EW | 4.64 | D | 0.146 | 45.96 | 121.47 | 0.32 | 8.1 | 23.98 |
| | TCU082-EW | 4.47 | D | 0.226 | 51.54 | 152.35 | 0.23 | 7.6 | 23.28 |
| | TCU102-EW | 1.19 | D | 0.304 | 87.16 | 163.13 | 0.29 | 2.6 | 14.93 |
| | TCU120-EW | 9.87 | C | 0.228 | 62.58 | 107.63 | 0.28 | 2.0 | 32.35 |
| | JEN-022 | 5.43 | D | 0.424 | 106.22 | 43.06 | 0.26 | 2.8 | 12.42 |
| | RRS-228 | 6.50 | D | 0.838 | 166.05 | 28.78 | 0.20 | 1.0 | 7.03 |
| | SCE-288 | 5.19 | D | 0.493 | 74.58 | 28.69 | 0.15 | 2.2 | 7.53 |
| | SCS-052 | 5.35 | D | 0.612 | 117.45 | 53.47 | 0.20 | 3.0 | 15.10 |
| | SYL-360 | 5.30 | D | 0.843 | 129.71 | 32.68 | 0.16 | 2.6 | 5.32 |
| Fling-step pulse | TCU052-NS | 1.84 | D | 0.488 | 220.64 | 723.27 (676.90) | 0.46 | 7.9 | 15.92 |
| | TCU052-EW | 1.84 | D | 0.356 | 182.96 | 506.73 (−443.10) | 0.52 | 5.6 | 16.78 |
| | TCU065-EW | 2.49 | D | 0.789 | 132.29 | 194.31(134.20) | 0.17 | 4.4 | 28.78 |
| | TCU067-EW | 1.11 | D | 0.499 | 97.26 | 186.16 (102.95) | 0.20 | 2.3 | 21.71 |
| | TCU068-NS | 3.01 | D | 0.365 | 291.94 | 867.76 (619.30) | 0.82 | 10.0 | 13.21 |
| | TCU068-EW | 3.01 | D | 0.505 | 279.88 | 709.11 (−567.30) | 0.57 | 9.4 | 12.36 |
| | TCU075-EW | 3.38 | D | 0.332 | 116.05 | 171.07 (120.00) | 0.36 | 4.2 | 26.92 |
| | TCU076-EW | 3.17 | D | 0.343 | 69.29 | 108.55 (87.56) | 0.21 | 3.7 | 29.68 |
| | TCU087-NS | 3.42 | C | 0.113 | 45.20 | 93.09 (−81.23) | 0.41 | 4.5 | 24.10 |
| | TCU128-EW | 9.08 | C | 0.144 | 60.58 | 145.39 (118.80) | 0.43 | 7.4 | 19.20 |
| Without pulse | TCU071-EW | 4.88 | D | 0.528 | 69.83 | 170.60 | 0.08 | 1.5 | 24.56 |
| | TCU072-EW | 7.87 | D | 0.476 | 85.51 | 223.86 | 0.18 | 0.8 | 21.92 |
| | TCU078-EW | 8.27 | D | 0.442 | 42.14 | 98.88 | 0.10 | 0.7 | 25.95 |
| | TCU079-EW | 10.95 | D | 0.589 | 64.49 | 173.20 | 0.11 | 0.8 | 24.24 |
| | TCU089-EW | 8.33 | C | 0.354 | 45.43 | 194.62 | 0.13 | 5.7 | 24.11 |
| | KAT-090 | 13.42 | D | 0.640 | 37.84 | 5.09 | 0.06 | 0.5 | 6.57 |
| | PKC-360 | 7.26 | D | 0.433 | 51.49 | 7.21 | 0.12 | 0.6 | 9.82 |
| | SPV-360 | 8.44 | D | 0.939 | 76.60 | 14.95 | 0.08 | 0.9 | 8.20 |
| | STC-180 | 12.09 | D | 0.477 | 61.48 | 22.06 | 0.13 | 1.3 | 10.61 |
| | TAR-360 | 15.60 | D | 0.990 | 77.62 | 30.45 | 0.08 | 0.7 | 12.66 |

*Note*: The data in the bracket correspond to the static displacement of near-fault ground motions with fling-step pulses.

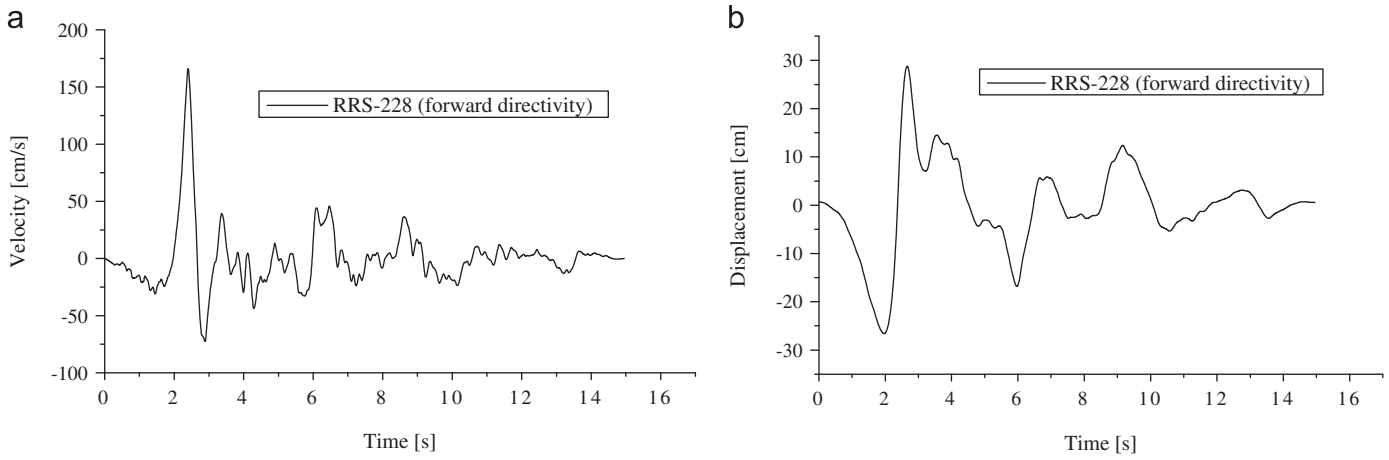


**Fig. 2.** Velocity and displacement time histories of near-fault ground motion RRS-228 with forward directivity pulse.

still beneficial to apply them to simulate and analyze the structural drift effects of real near-fault ground motions. Moreover, the use of simple pulses can offer some insights in distinguishing the seismic responses of typical structures to variation in pulse characteristics. Makris and Chang [21] suggested three kinds of simple velocity pulses such as Type-A, -B, and -$C_n$ for characterizing the near-fault pulse-like ground motions. Type-A can represent the one-sided (non-reversing) fling-step pulse with static offset at the end of the displacement time history and Type-B and Type-$C_n$ represent the two-sided (reversing) forward directivity pulses [17,28]. In practice, the waveform of impulsive ground motions with fling-step effects in Table 1 resembles Type-A model and the waveform of impulsive ground motions with forward directivity effects resembles Type-B and -$C_n$ models.

### 4.1. Simple pulse models and their response spectra

The acceleration, velocity and displacement time histories governing the Type-A pulse are written as follows[21,28]:

$$a_g^A = \omega_p \frac{V_p}{2}\sin(\omega_p t) \quad v_g^A = \frac{V_p}{2} - \frac{V_p}{2}\cos(\omega_p t), \quad d_g^A = \frac{V_p}{2}t - \frac{V_p}{2\omega_p}\sin(\omega_p t), \quad 0 \le t \le T_p \tag{9}$$

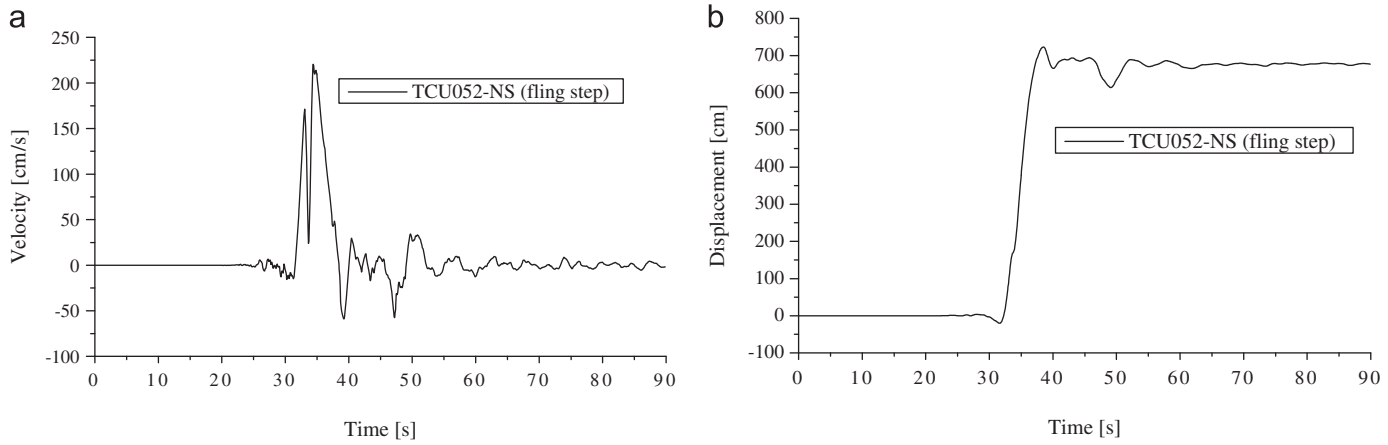


**Fig. 3.** Velocity and displacement time histories of near-fault ground motion TCU052-NS with fling-step pulse.

where $V_p$ represents the amplitude of pulse velocity, $T_p$ denotes the pulse period and $\omega_p=2\pi/T_p$. The Type-B pulse is expressed as

$$a_g^B=\omega_p V_p\cos(\omega_p t),\quad v_g^B=V_p\sin(\omega_p t),\quad d_g^B=\frac{V_p}{\omega_p}-\frac{V_p}{\omega_p}\cos(\omega_p t),\quad 0\le t\le T_p \tag{10}$$

For the Type-C$_n$ pulse, the velocity and displacement histories display one or more long duration cycles. An $n$+half cycles for Type-C$_n$ are defined by

$$a_g^C=\omega_p V_p\cos(\omega_p t+\varphi),\quad v_g^C=V_p\sin(\omega_p t+\varphi)-V_p\sin(\varphi)$$

$$d_g^C=-\frac{V_p}{\omega_p}\cos(\omega_p t+\varphi)-V_p t\sin(\varphi)+\frac{V_p}{\omega_p}\cos(\varphi),\quad 0\le t\le\left(n+\frac{1}{2}-\frac{\varphi}{\pi}\right)T_p \tag{11}$$

where the phase angle $\varphi$ is determined by imposing zero ground displacement at the end of the pulse duration.

The time histories and 5% damped elastic pseudo-acceleration spectra of Type-A, -B and -C$_2$ ($\varphi=0.041\pi$) pulses are shown in Fig. 4. The parameters of simple pulses in Fig. 4 are taken as: $V_p=100$ cm/s, $T_p=4$ s; Type-A, $PGV=100$ cm/s, $PGA=78.5$ gal; Type-B, $PGV=100$ cm/s, $PGA=157.1$ gal and Type-C$_2$, $PGV=112.8$ cm/s, $PGA=157.1$ gal. It is noted that the three types of simple pulses have the same or close $PGV$, and each type of pulse with $T_p=2$ s rather than $T_p=4$ and 6 s presents the largest $PGA$. Hence, the acceleration response of simple pulses corresponding to $T_p=2$ s is largest near the period 2 s of SDOF system. Moreover, the spectral acceleration of idealized pulses attains the maximum at the vicinity of period $T=T_p$, which verifies the resonant phenomenon [24]. Finally, it should be pointed out that the pulse models in Eqs.(9)–(11) attempt to represent velocity time history of near-fault records. In this case $V_p$ would correspond to $PGV$, which is true for Type-A and -B pulse models. However, this is not the case for Type-C$n$ pulse model. Since $PGV$ is a good indicator of damage potential in the near-fault ground motions, it is important to understand the resemblance or difference between $V_p$ and $PGV$.

In addition, the velocity and displacement time histories of ground motions RRS-228 and TCU052-NS are shown in Figs. 1 and 2, respectively, and the time histories of simple pulses are displayed in Fig. 4. By comparison, it is found that the forward directivity pulse Type-B has the similar velocity and displacement time series to ground motion RRS-228. Meanwhile, the fling-step pulse Type-A has the similar velocity and displacement time series to ground motion TCU052-NS. But the acceleration time series between them demonstrate their difference, which is actually the common limitation for the idealized pulses [21,23–25,28]. Moreover, the idealized pulses can generally characterize the coherent component of near-fault ground motions, and cannot replicate the incoherent (high-frequency) seismic radiation. Therefore, the spectral responses of ideal pulses can represent the seismic responses of long-period structures with fundamental period longer than pulse period ($T>T_p$), instead of those of short-period structures [25].

### 4.2. Generalized interstory drift spectra of simple pulses

According to the generalized interstory drift spectrum introduced in Section 2, the IDR of simple pulses is computed. Fig. 5 illustrates the generalized drift spectra of Type-A, -B and -C$_2$ with different $T_p$. Similar to elastic response spectra in Fig. 4, the IDR demands of simple pulses are largest near the period $T=T_p$, which indicate that there is a quasi-resonant phenomenon in the interstory drift spectra. Moreover, the IDR of the simple pulses with $T_p=2$ s is larger than $T_p=4$ and 6 s in the short and medium periods and the IDR of the simple pulses with $T_p=4$ s is the largest about the period 4 s. Thus, the IDR of the simple pulses with $T_p=6$ s is the largest in the period greater than 6 s. On the other hand, the amplitude and the form of drift spectra of three types of simple pulses with the same $V_p$ and $T_p$ display significant difference. The IDR of Type-C$_2$ model is the largest and the IDR of Type-A is the smallest in the whole period, which means that the simple pulses with forward directivity produce more intense drift demands, and the pulses with several cycles also generate larger drift ratios [24].

One important advantage of generalized interstory drift spectrum lies in that the drift spectral analysis can offer the maximum dynamic responses (i.e. drift ratio, displacement, acceleration etc.) of equivalent beam along the height. Fig. 6 demonstrates the IDR along the dimensionless beam height for representative fundamental periods ($T_1=0.3$, 1.0 and 3.0 s) and different stiffness ratios ($\alpha=0$, 20 and 650) under simple pulses Type-A, -B and -C$_2$ with $T_p=2$ s and $V_p=100$ cm/s, respectively. It is expected that the IDR of building under these simple pulses corresponding to fundamental period $T_1=2.0$ s is larger than that of the three representative periods owing to resonant effect.

From Fig. 6, it is observed that for pure flexural beam representing flexural buildings ($\alpha=0$), the maximum IDR occurs at the top story of buildings; for the pure shear system ($\alpha=650$),

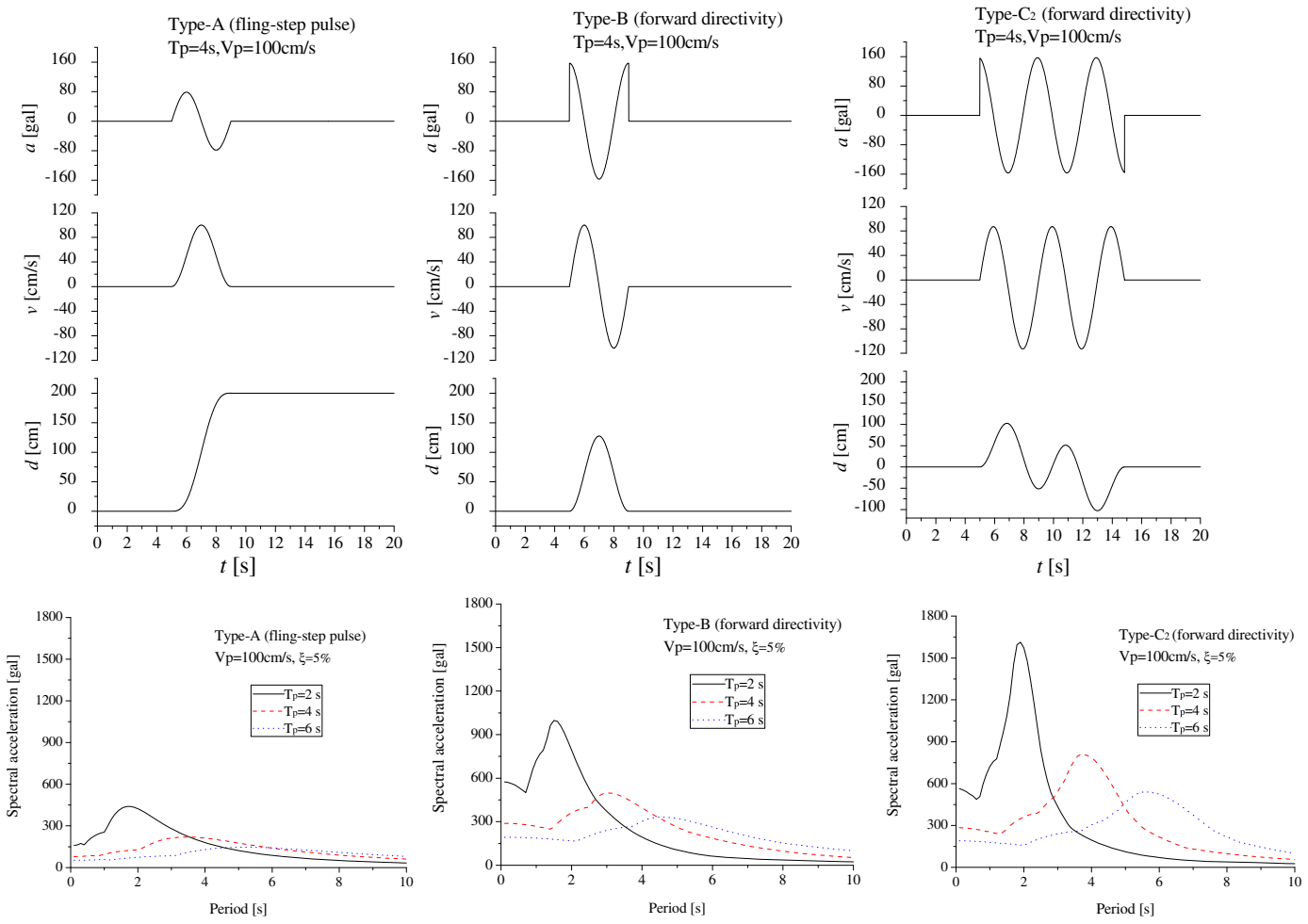


**Fig. 4.** Time histories and elastic acceleration spectra of Type-A, -B and -$C_2$.

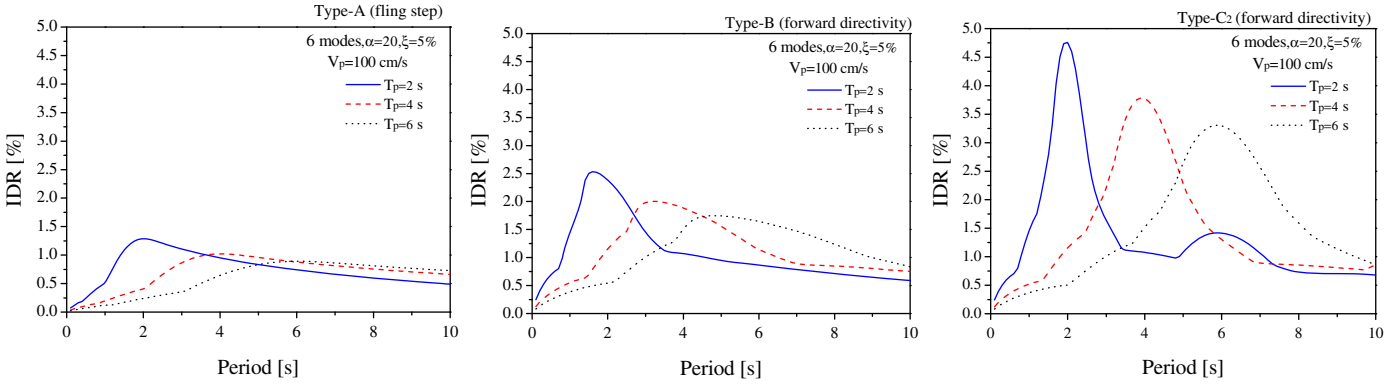


**Fig. 5.** Generalized interstory drift spectra of Type-A, -B and -$C_2$ with different $T_p$.

the maximum IDR occurs at the ground story and for the combined system ($\alpha=20$), the maximum IDR presents at the lower level of buildings. Furthermore, the deformation mode of Type-A pulse with fling-step differs from that of Type-B and especially Type-$C_2$ with forward directivity when the fundamental period of the system is longer ($T=3.0$ s). For instance, for combined shear-flexural system characterizing the reinforced concrete (RC) moment-resisting frame building ($\alpha=20$, $T=3.0$ s) [11], the maximum $IDR=1.60\%$ of Type-$C_2$ pulse occurs at the normalized height $z/H=0.35$, but the largest $IDR=1.08\%$ of Type-A pulse occurs at the lower height $z/H=0.18$. It appears that the forward directivity pulses can amplify the contribution of higher modes of system, and the fling-step pulses can excite a primarily first-mode response, which agrees with the observation in the reference [17]. However, this phenomenon needs to be investigated when subjected to actual near-fault pulse-like ground

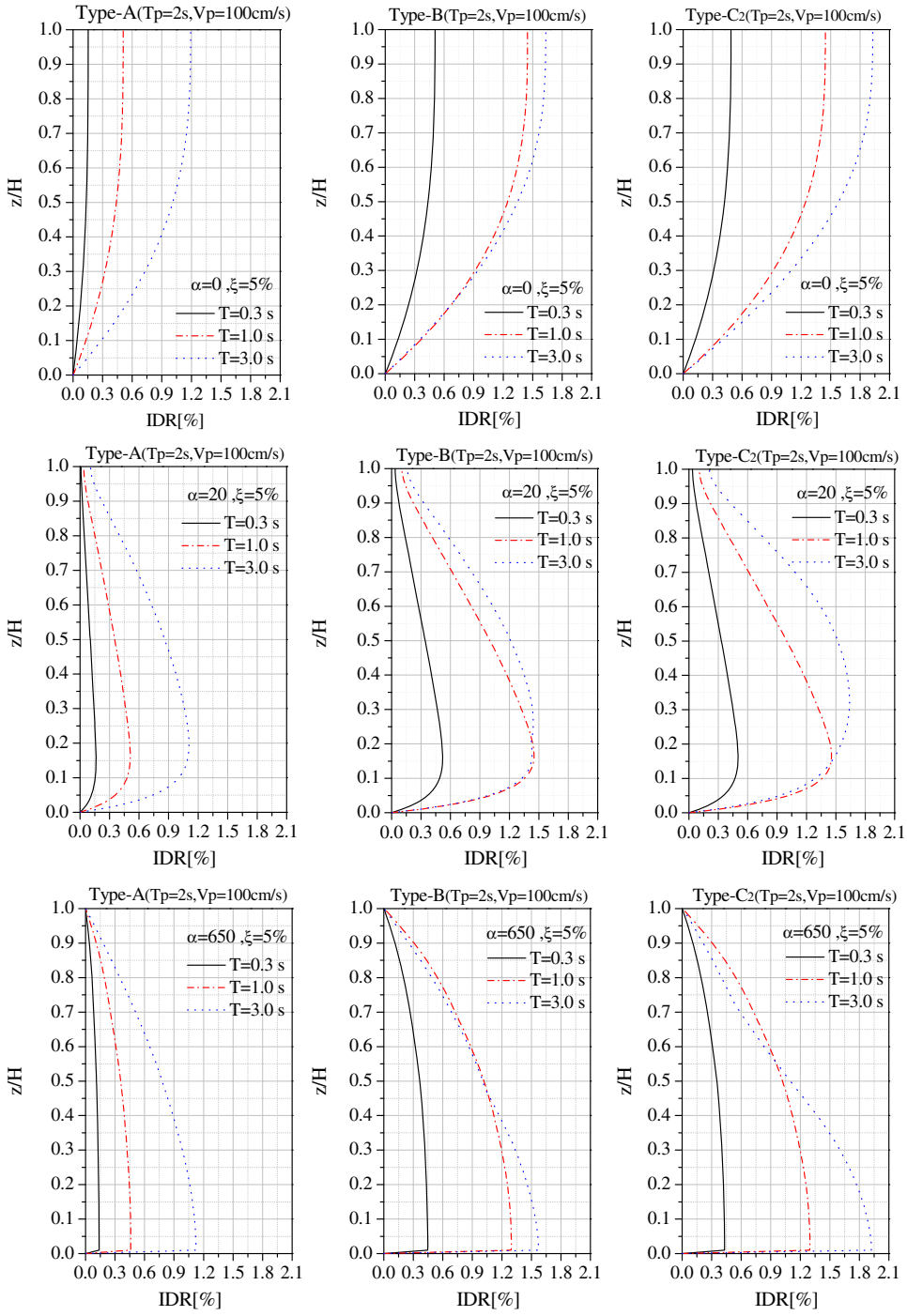


**Fig. 6.** Interstory drift ratio along dimensionless height for fundamental periods $T=0.3$, 1.0 and 3.0 s under simple pulses Type-A (fling tep), -B and -$C_2$ (forward directivity).

motions. Moreover, the cause responsible for the above phenomenon should have to be explored theoretically. The next section devotes to reveal the fundamental reason in terms of the distinct property of near-fault impulsive ground motions and generalized drift spectral analysis.

### 4.3. Analysis on IDR distribution along height based on generalized drift spectrum

Firstly, we recall the formula (7) to examine the contribution of each mode of vibration to the IDR of continuous beam. It is seen from Eq. (7) that the IDR depends on the product of the modal participation factor $\Gamma_i$, the derivative of the mode shape $\phi_i'(x)$ and the relative displacement response of a SDOF system $D_i(t)$. If the fundamental period of the building is known, the periods of vibration of higher modes can be computed as

$$T_i = T_1 \frac{\gamma_1}{\gamma_i} \sqrt{\frac{\alpha^2+\gamma_1^2}{\alpha^2+\gamma_i^2}} \tag{12}$$

where the eigenvalue $\gamma_i$ of the $i$th mode of vibration can be obtained by solving a characteristic equation [11]. For a

continuum model with uniform mass distribution, the modal participation factors $\Gamma_i$ can be given by [11]

$$\Gamma_i = \frac{\int_0^1 \phi_i(x)dx}{\int_0^1 \phi_i^2(x)dx} \tag{13}$$

It can be seen that the product of the modal participation factor and the derivative of the mode shape $\Gamma_i\phi_i'(x)$ only relies on the lateral stiffness ratio $\alpha$ of building, and it has no relation with ground excitation at all. Nevertheless, the modal displacement $D_i(t)$ depends on both the modal period $T_i$ and the ground acceleration $\ddot{u}_g(t)$. In other words, $D_i(t)$ depends on the characteristic of ground motion given a specific stiffness ratio. Hence, IDR is also related to the property of near-fault ground motions via the modal displacement $D_i(t)$. Moreover, the IDR is approximately equal to the product of modal peak displacement $D_i$ ($=\max|D_i(t)|$) and $\Gamma_i\phi_i'(x)$ in a simplified way according to Eq.(7), namely

$$\mathrm{IDR}(x) \approx \frac{1}{H}\sum_{i=1}^{m} \Gamma_i\phi_i'(x)D_i \tag{14}$$

Fig. 7 shows the product $\Gamma_i\phi_i'(x)$ of the first four modes of vibration depending on lateral stiffness ratios ($\alpha$=0, 3, 7, 20 and 650). It is easily seen that the influence of stiffness ratio on the product $\Gamma_i\phi_i'(x)$ is significant. The stiffness ratio has also a remarkable effect on the amplitude and location of the maximum value of the product along dimensionless height. For the first mode, the influence of $\alpha$ is particularly large near the top and bottom of the structure, while at the middle height the influence of $\alpha$ is moderate. Examination of this figure indicates that for large values of the lateral stiffness ratio ($\alpha \geq 20$), the IDR distribution is like the shape of the letter '*D*', and the maximum contributions of the first mode to the IDR will tend to occur toward the bottom of the building, while for small values of stiffness ratio ($\alpha \leq 3$) the maxima tend to present in the upper portion of the building. It can also be seen that, as expected, for the shear beam ($\alpha$=650) the contribution of the first mode attains its maximum at the base of the building, while for a pure flexural beam ($\alpha$=0) the contribution of the first mode has its maximum at the top. For higher modes, the influence of $\alpha$ on the amplitude and location of the maximum value of the product $\Gamma_i\phi_i'(x)$ is also noticeable [11]. In contrast to Fig. 7, the results in Fig. 6 demonstrate that the contribution of the first mode to IDR is primary, and the contributions of higher modes to IDR are secondary.

Meanwhile, Fig. 8 illustrates the 5% damped elastic displacement spectra of three types of simple pulses with $T_p$=2 s and $V_p$=100 cm/s. Table 2 presents the modal peak displacement of shear-flexural beam ($\alpha$=20) with fundamental periods ($T_1$=3.0, 1.0 and 0.3 s) subjected to simple pulses. The number of modes of vibration is set as four ($m$=4). According to Eq.(12), if the fundamental period of continuous beam is taken as $T_1$=3.0 s, then the modal periods are equal to: $T_2$=0.98 s, $T_3$=0.56 s and $T_4$=0.38 s. The percentage of modal peak displacement of shear-flexural beam is also listed in the bracket in Table 2. For this case of shear-flexural beam ($\alpha$=20, $T_1$=3.0 s), the modal peak displacement $D_i$ of beam model under forward directivity pulse Type-$C_2$ is the largest, while the modal peak displacement $D_i$ of beam model under fling-step pulse Type-A is the smallest. Furthermore, the modal IDR is approximately equal to the product of $\Gamma_i\phi_i'(x)$ and the modal peak displacement $D_i$. Therefore, the maximum IDR along the dimensionless height under Type-$C_2$ is larger than that under Type-A as shown in Fig. 6. On the other hand, for the first mode, the percentage (88.1%) of modal peak displacement of shear-flexural beam under fling-step pulse Type-A is the largest. Consequently, the contribution of the

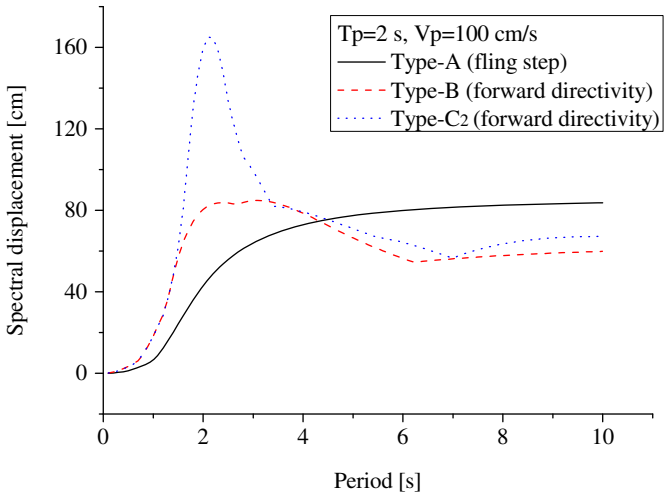


**Fig. 8.** Elastic displacement spectra of simple pulses with $T_p$=2 s and $V_p$=100 cm/s.

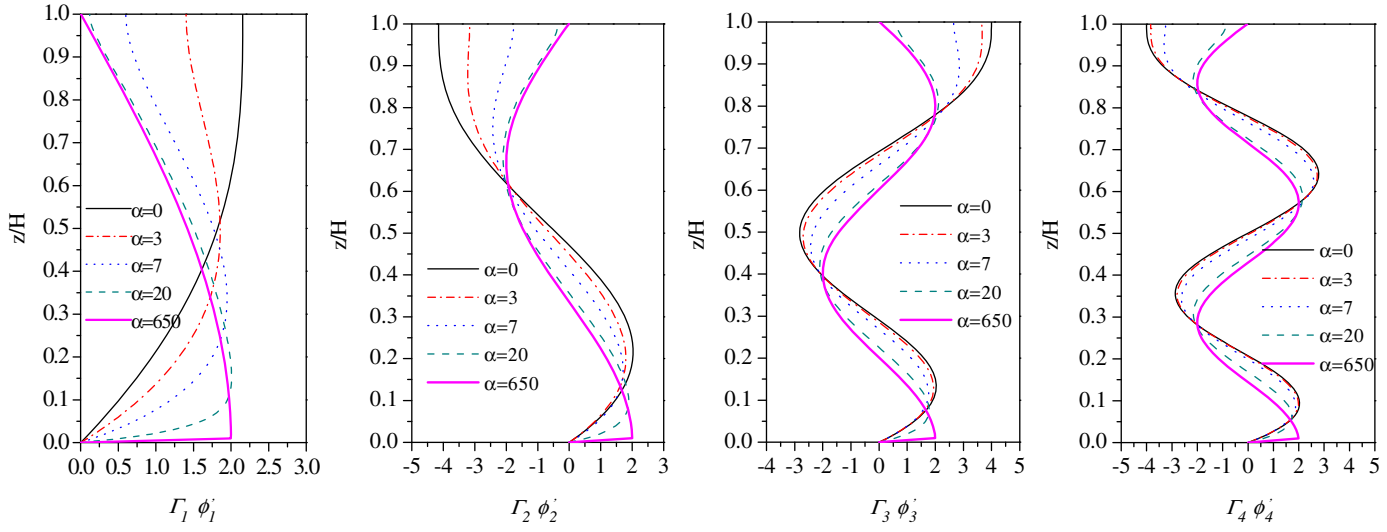


**Fig. 7.** Effect of $\alpha$ on the product of modal participation factor and derivative of mode shape.

**Table 2**
Modal peak displacement of shear-flexural beam ($\alpha=20$) with fundamental periods ($T_1=3.0$, 1.0 and 0.3 s) subjected to simple pulses ($D_i$, cm).

| | $T_1=3.0$ s | | | $T_1=1.0$ s | | | $T_1=0.3$ s | | |
|---|---|---|---|---|---|---|---|---|---|
| | Type-A | Type-B | Type-$C_2$ | Type-A | Type-B | Type-$C_2$ | Type-A | Type-B | Type-$C_2$ |
| $D_1$ | 63.91 (88.1%) | 84.78 (77.5%) | 99.35 (80.3%) | 6.44 (89.2%) | 18.28 (86.8%) | 18.31 (87.3%) | 0.39 (81.3%) | 1.28 (79.0%) | 1.24 (79.0%) |
| $D_2$ | 6.42 (8.8%) | 18.12 (16.6%) | 18.26 (14.7%) | 0.51 (7.1%) | 2.07 (9.8%) | 1.96 (9.3%) | 0.04 (8.3%) | 0.14 (8.6%) | 0.14 (8.9%) |
| $D_3$ | 1.62 (2.2%) | 4.30 (3.9%) | 4.18 (3.4%) | 0.22 (3.0%) | 0.56 (2.7%) | 0.55 (2.6%) | 0.03 (6.3%) | 0.11 (6.8%) | 0.11 (7.0%) |
| $D_4$ | 0.63 (0.86%) | 2.17 (2.0%) | 1.93 (1.5%) | 0.05 (0.7%) | 0.15 (0.7%) | 0.15 (0.7%) | 0.02 (4.1%) | 0.09 (5.6%) | 0.08 (5.1%) |

*Note*: The data in the bracket denote the percentage of modal peak displacement of shear-flexural beam under simple pulses.

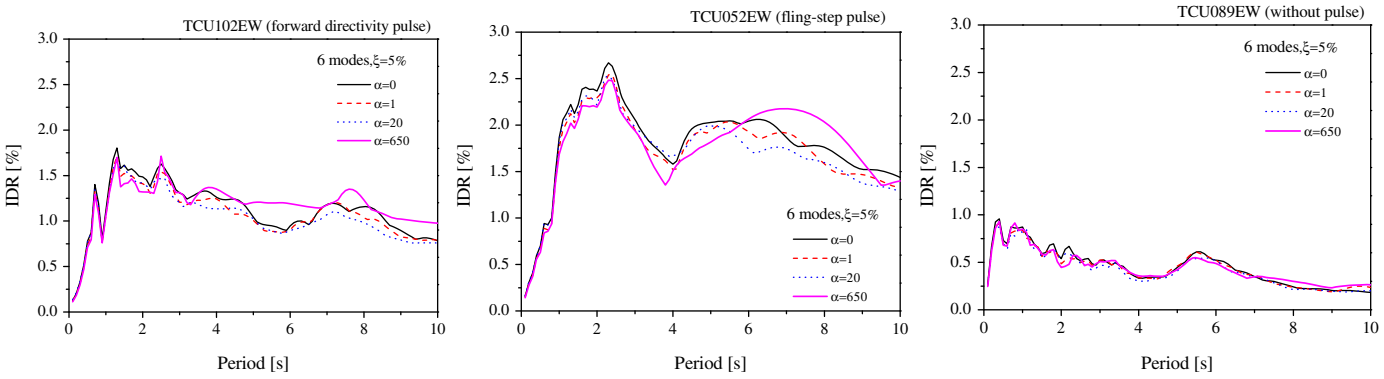


**Fig. 9.** Effect of stiffness ratio $\alpha$ on generalized interstory drift spectrum under representative ground motions.

first mode to IDR under Type-A is the largest, and the location ($z/H=0.18$) of the maximum IDR along height of building under fling-step pulse Type-A is lower than that of ($z/H=0.35$) under forward directivity pulse Type-$C_2$, as observed in Section 4.2. Additionally, the large percentage ($>75\%$) of modal peak displacement of shear-flexural beam for the first mode under simple pulses in Table 2 explains the cause why the contribution of the first mode to IDR is primary. To sum up, the modal peak displacement of shear-flexural beam under ground excitations determines the maximum IDR and the IDR distribution along the height of the structure to a great degree.

## 5. IDR distribution of buildings under representative near-fault ground motions

Actually, the model parameters (lateral stiffness ratio $\alpha$, damping ratio $\xi$ and number of modes $m$ ) of buildings (which are equivalently taken as shear-flexural beams) affect the generalized interstory drift spectrum subjected to three representative near-fault ground motions in Table 1 with the close *PGA*, i.e. TCU102-EW (forward directivity pulse, *PGA*=0.304 g ), TCU052-EW (fling-step pulse, *PGA*=0.356 g) and TCU089-EW (without pulse, *PGA*=0.354 g) from Chi-Chi earthquake, Taiwan.

According to Eqs.(7) and (8) and considering the first six modes of vibration ($m=6$), Fig. 9 demonstrates the generalized interstory drift spectrum for 5% damped shear-flexural beam with four typical values of $\alpha$ (0, 1, 20 and 650) subjected to three typical ground motions. For a given fundamental period, the total height of the model in Eq.(7) is calculated using the relationship suggested for steel moment-resistant frames in the 1997 UBC code, namely, $T_1=0.0853H^{0.75}$[11]. It is shown that for the systems with fundamental period less than 1.2 s, the influence of $\alpha$ on the interstory drift spectrum is negligible. But for the systems with longer period, the influence of $\alpha$ on the interstory drift demands becomes large, particularly for TCU102-EW ground motion with forward directivity pulse and TCU052-EW ground motion with fling-step pulse. On the other hand, comparing Fig. 9 with Fig. 5, it is observed that the forms of generalized interstory drift spectra are different. The generalized interstory drift spectrum of TCU052-EW with fling-step effect presents more peaks than that of ideal pulse Type-A in Fig. 5, in which the spectral shape is more smooth. Similarly, the generalized drift spectrum of TCU102-EW with forward directivity has more peaks than that of the simple pulse Type-B in Fig. 5.

In terms of the generalized interstory drift spectral analysis of three representative ground motions, the influence of damping ratio and the number of modes on interstory drift spectrum of shear-flexural beam are basically in agreement with the findings of Miranda and Akkar [11]. Herein, the IDR distribution over the height of buildings is emphasized to investigate.

Fig. 10 shows the IDR distribution of buildings along the dimensionless height for different fundamental periods ($T=0.3$, 1.0 and 3.0 s) and different stiffness ratios ($\alpha=0$, 20 and 650) subjected to three typical ground motions, respectively. It can be seen that the maximum IDR shifts from the upper half to the lower half of buildings with an increase in the lateral stiffness ratio $\alpha$. Further, the long-period structures under impulsive ground motions suffer more intensive IDR, which is consistent with the previous observations [22,24]. Meanwhile, for the moment-resisting frame building ($\alpha=20$, $T=3.0$ s) [11], the maximum *IDR*=1.20% of the TCU102-EW with forward directivity pulse presents at the height $z/H=0.20$. But the largest *IDR*=1.99% of the TCU052-EW with fling-step pulse occurs at the height $z/H=0.16$ slightly lower than the former height, which is similar to the observations in Section 4.2, indicating that the ground motion with fling-step pulse excites the first-mode response more than the ground motion with forward directivity pulse.

Fig. 11 displays the 5% damped displacement spectra of three typical near-fault ground motions, which are different from the displacement spectra of idealized simple pulses in Fig. 8. Table 3 presents the modal peak displacement of buildings ($\alpha=20$) with

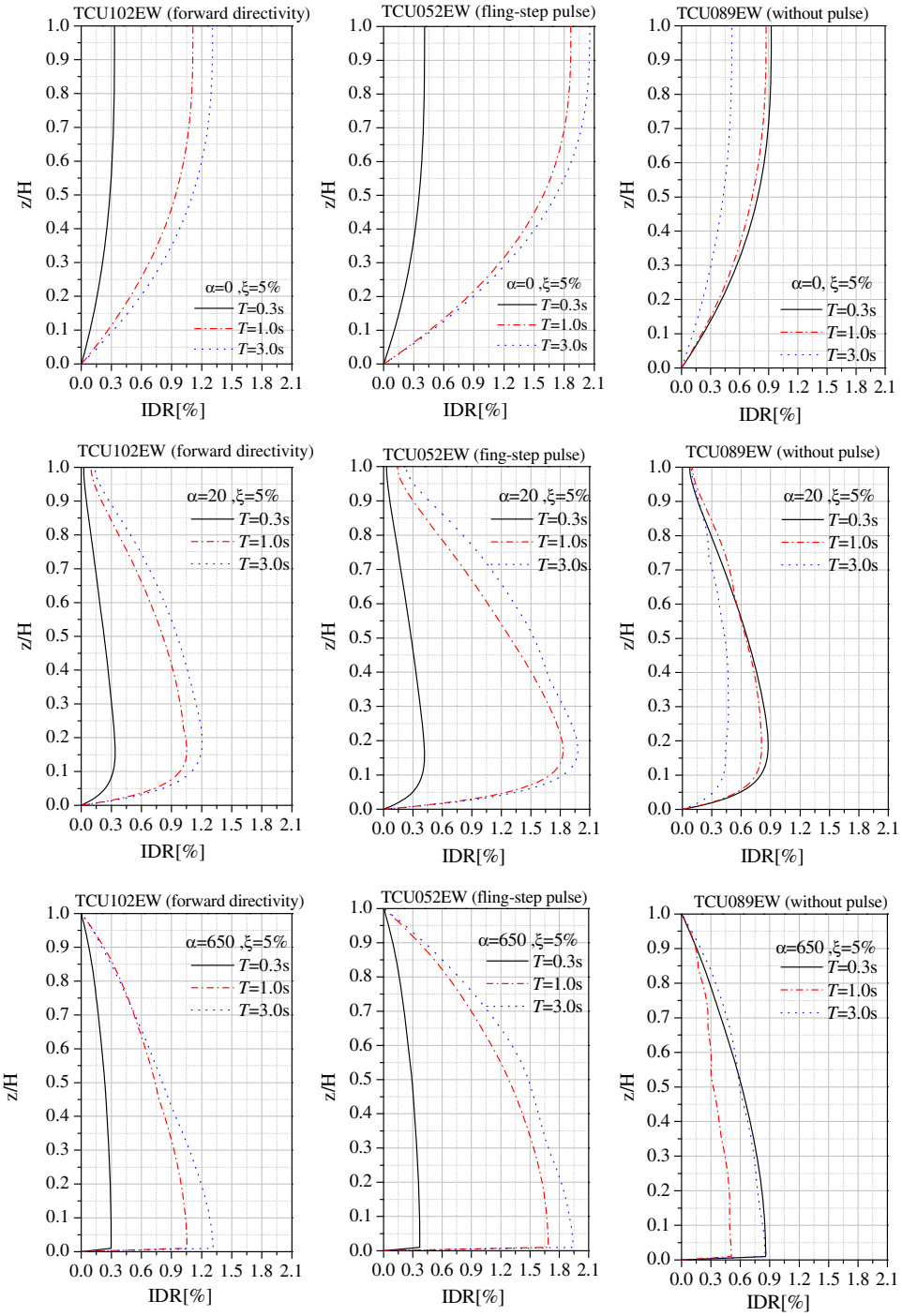


**Fig. 10.** IDR distribution of buildings with fundamental periods $T=0.3$, 1.0 and 3.0 s under representative ground motions with similar *PGA*.

fundamental periods ($T_1=3.0$, 1.0 and 0.3 s) subjected to typical ground motions (TCU102-EW, TCU052-EW and TCU089-EW). As pointed out in Section 4.3, the modal peak displacement of continuous beam subjected to ground excitations determines the IDR response of structure to a large extent. For the moment-resisting frame buildings ($\alpha=20$, $T_1=3.0$ s), the modal peak displacement $D_i$ of buildings under ground motion with fling-step pulse TCU052-EW is the largest, while the modal peak displacement $D_i$ of buildings under non-pulse motion TCU089-EW is the smallest. Thus, the maximum IDR along the dimensionless height under TCU052-EW is larger than that under TCU089-EW and TCU102-EW as shown in Fig. 10. On the other hand, for the first mode, the percentage (78.2%) of the modal peak displacement of buildings under TCU052-EW is also the largest. Accordingly, the contribution of the first mode to IDR subjected to TCU052-EW is the largest, and the location ($z/H=0.16$) of the maximum IDR along height of building under ground motion with fling-step pulse TCU052-EW is lower than that ($z/H=0.20$) under forward directivity pulse TCU102-EW. In addition, the large percentage of modal peak displacement of buildings for the first mode under typical ground motions in Table 3 makes the contribution of the first mode to IDR important.

Although *PGA* is a widely-used intensity measure parameter of earthquake ground motions, for near-fault ground motions *PGV* is

also an appropriate intensity index especially to medium-period structural systems [29]. Accordingly, three near-fault ground motions with similar *PGV* , namely, TCU120-EW, *PGV*=62.58 cm/s; TCU076-EW, *PGV*=69.29 cm/s and TCU079-EW, *PGV*=64.49 cm/s are chosen as input to compare their seismic effects. Fig. 12 illustrates the IDR distribution of buildings over the dimensionless height for different fundamental periods and stiffness ratios subjected to three ground motions with the close *PGV*, separately. For the moment-resisting frame building ($\alpha$=20, $T$=3.0 s), the maximum *IDR*=0.75% of TCU120-EW with forward directivity pulse occurring at a height $z/H$=0.17. Whereas, the largest *IDR*=0.79% of TCU076-EW with fling-step pulse presenting at the height $z/H$=0.16 slightly lower than the former height, also indicating that the ground motion with fling-step pulse can excite the first-mode response more than ground motion with forward directivity pulse. Fig. 13 demonstrates the 5% damped displacement spectra of three near-fault ground motions with similar *PGV*. Furthermore, based on Fig. 13 and simplified formulation Eq.(14), we can explain the above phenomenon. Nevertheless, the different waveforms and amplitudes of acceleration time histories of the three ground motions cause different IDR distributions of buildings shown in Fig. 12 from Fig. 10.

## 6. Interstory drift spectral analysis of three groups of near-fault ground motions

In the past years, the effects of characteristic of near-fault ground motions on dynamic responses of building systems were mainly investigated by time history analysis [17–24]. In this section, the IDR demands of buildings subjected to three distinct groups of near-fault ground motions with forward directivity pulses, fling-step pulses and without pulse listed in Table 1 are examined based on generalized drift spectra.

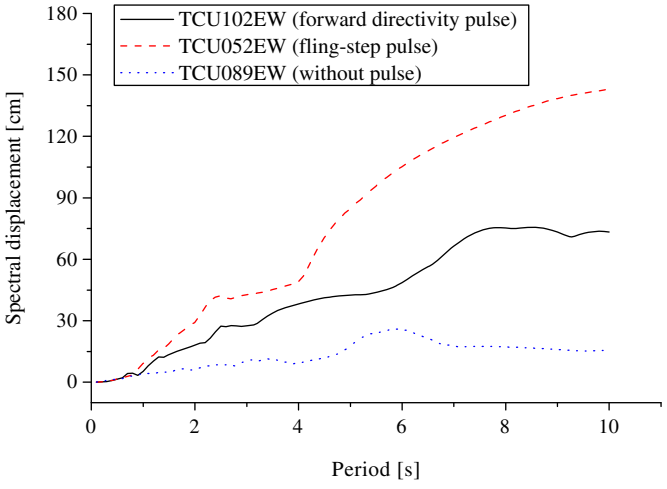


**Fig. 11.** Elastic displacement spectra of three typical near-fault ground motions with similar *PGA*.

### 6.1. Generalized drift spectra of three groups of near-fault ground motions

Figs. 14–16 show the 5% damped generalized interstory drift spectra of three groups of near-fault ground motions with six vibration modes ($m$=6) and four different lateral stiffness ratios ($\alpha$=0, 1, 20 and 650). Some observations are obtained as follows:

(1) Both the form and amplitude of generalized drift spectra are similar for different lateral ratios $\alpha$ of shear-flexural beam. For example, for the ground motions with forward directivity pulses, the difference in drift spectra among lateral stiffness ratios is very small except in the range of long period for $\alpha$=650. Furthermore, the spectral variance among all records in three groups of ground motions differs from each other significantly. The spectral dispersion of near-fault ground motions with fling-step pulses is the largest especially in the long-period range. Whereas, the spectral dispersion of ground motions without pulse is the smallest indicating that the dispersion among non-pulse ground excitations is small.

(2) For three groups of ground motions with different characters, the discrepancy of generalized drift spectra is remarkable. As for near-fault ground motions with forward directivity, the IDR in drift spectra is larger in the range of short- and medium period, and the spectral predominant period is between 0.5 and 2.2 s. In the long-period range, the IDR decreases slowly with the increase in fundamental period. Furthermore, the spectral form of non-pulse ground motions is similar to that of ground motions with forward directivity pulses, but its predominant period is shortened in the interval of 0.3 and 2.0 s. In the short period, the IDR increases to the vertex sharply. Then, it decays gradually. The IDR of non-pulse ground motions is less than 1.0% except in the short period. But in contrast with the former two kinds of drift spectra, the spectral predominant period of ground motions with fling-step pulses is prolonged. Individually, when the structural period is larger than 6.0 s, the spectral IDR of ground motion TCU068-NS is still large and reaches to 2.5% where its predominant period is 8.0 s.

(3) As shown in Fig. 14, the IDR under three ground motions (RRS-228, SCS-052 and SYL-360) with forward directivity pulses exceed 2.5% in the short period and medium period. Moreover, as illustrated in Fig. 15, the IDR under several ground motions (TCU065-EW, TCU052-NS, TCU068-NS, TCU068-EW and TCU052-EW) with fling-step pulses exceeding 2.5% in the medium and long periods. However, as illustrated in Fig. 16, the IDR under one ground motion

**Table 3**
Modal peak displacement of buildings ($\alpha$=20) with fundamental periods ($T_1$=3.0, 1.0 and 0.3 s) subjected to typical near-fault ground motions ($D_i$, cm).

| | $T_1$=3.0 s | | | $T_1$=1.0 s | | | $T_1$=0.3 s | | |
|---|---|---|---|---|---|---|---|---|---|
| | TCU102-EW | TCU052-EW | TCU089-EW | TCU102-EW | TCU052-EW | TCU089-EW | TCU102-EW | TCU052-EW | TCU089-EW |
| $D_1$ | 27.62 (77.7%) | 42.73 (78.2%) | 10.62 (59.9%) | 5.40 (90.3%) | 9.17 (92.1%) | 4.19 (73.4%) | 0.33 (80.5%) | 0.41 (83.7%) | 0.90 (85.7%) |
| $D_2$ | 5.40 (15.2%) | 9.12 (16.7%) | 4.13 (23.3%) | 0.43 (7.2%) | 0.58 (5.8%) | 1.04 (18.2%) | 0.03 (7.3%) | 0.03 (6.1%) | 0.06 (5.7%) |
| $D_3$ | 1.82 (5.1%) | 1.95 (3.6%) | 1.64 (9.3%) | 0.11 (1.8%) | 0.16 (1.6%) | 0.34 (5.9%) | 0.03 (7.3%) | 0.03 (6.1%) | 0.05 (4.8%) |
| $D_4$ | 0.72 (2.0%) | 0.84 (1.5%) | 1.33 (7.5%) | 0.04 (0.7%) | 0.05 (0.5%) | 0.14 (2.5%) | 0.02 (4.9%) | 0.02 (4.1%) | 0.04 (3.8%) |

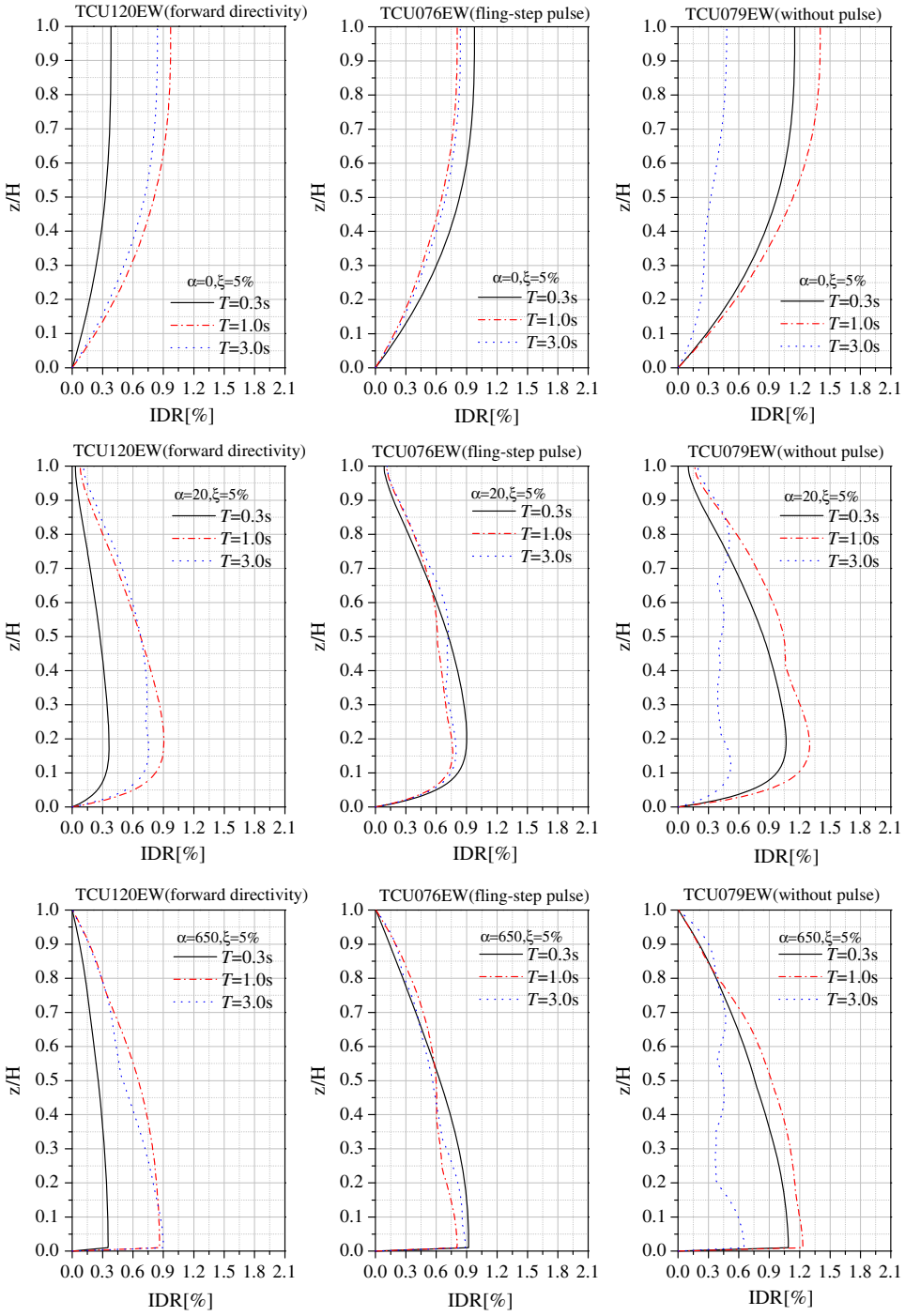


**Fig. 12.** IDR distribution of buildings with fundamental periods $T=0.3$, 1.0 and 3.0 s under near-fault ground motions with similar *PGV*.

(TAR-360) without pulse attaining 2.5% in the short period. These observations demonstrate that the impulsive ground motions have larger damage potential than the non-pulse ground motions especially for the medium- and long-period systems.

The generalized drift spectra in Figs. 14–16 are averaged, and the mean drift spectra of three groups of near-fault ground motions with four different lateral stiffness ratios ($\alpha=0$, 1, 20 and 650) are presented in Fig. 17, respectively. It can be seen that the influence of stiffness ratio $\alpha$ on the average IDR is small. In particular, it is negligible in the short-period range. The average IDR attain 1.5% in respective periods for the three groups of records implying that the building could suffer heavy damage. As expected, the average IDR spectra among three groups of ground motions have significant discrepancy. In the short period, three mean spectra increase sharply to peak especially for non-pulse ground motions. Then, the mean IDR spectra of impulsive ground motions present a flat to keep large drift ratios. For ground motions with forward directivity pulses, the period corresponding to the flat is in the range 1.3–2.5 s. Moreover, for ground motions with fling-step pulses, the period corresponding to the flat is prolonged to the range 1.1–8.0 s and their average IDRs are remarkably larger than those under ground motions with forward directivity pulses for the long-period systems

($T > 3.0$ s). Essentially, the abundant long-period components of impulsive near-ground motions cause this phenomenon. Nevertheless, for non-pulse ground motions, the mean IDR spectra do not have such a flat. Its average IDR goes through the peak at the predominant period 0.6 s, and then decays quickly. When the period is longer than 3.0 s, it decreases slowly.

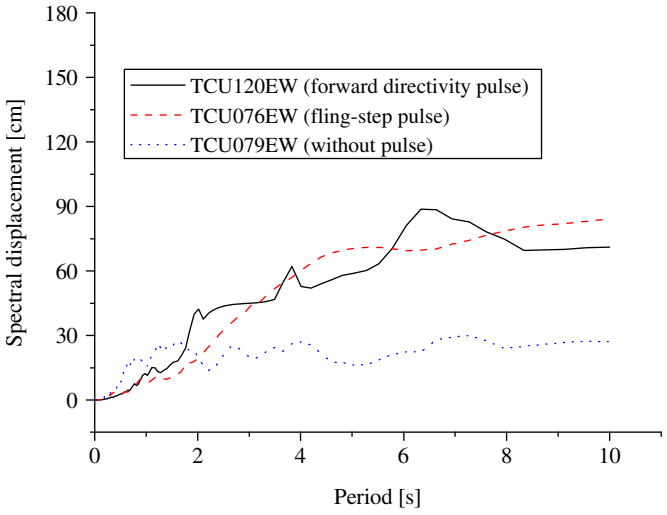


**Fig. 13.** Elastic displacement spectra of three near-fault ground motions with similar *PGV*.

Finally, it is noted that the spectral averages of IDR in Fig. 17 are computed for narrow magnitude range. Because the ground motions of the Chi-Chi and Northridge earthquakes with magnitudes of 7.6 and 6.7 are used separately, the average IDR barely considers the possible effect of magnitude on the interstory drift demands. Meanwhile, the aforementioned observations are valid for dense-to-stiff soil sites, e.g. site classes C and D.

### 6.2. IDR distribution of buildings under three groups of near-fault ground motions

Fig. 18 presents the mean IDR distribution of buildings with $\alpha=20$ and different fundamental periods ($T=0.3$, 1.0 and 3.0 s) subjected to three groups of ground motions, respectively. It is found that the deformation mode of mean IDR varies from short- to long-period system under different groups of near-fault motions. Furthermore, for the moment-resisting frame building ($\alpha=20$, $T=3.0$ s), the largest mean $IDR=1.03\%$ under ground motions with forward directivity

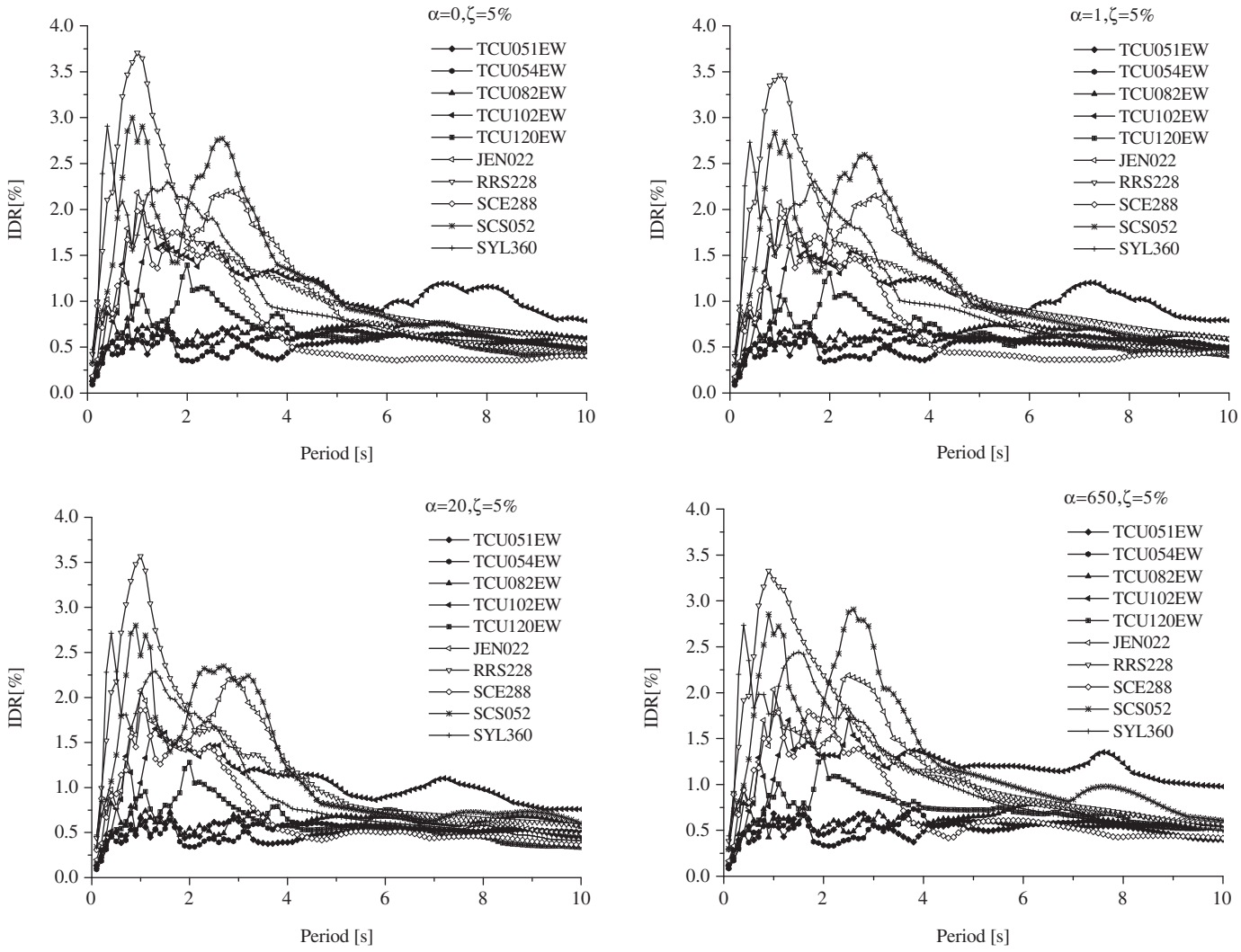


**Fig. 14.** Interstory drift spectrum of near-fault ground motions with forward directivity pulses for $\alpha=0$, 1, 20 and 650.

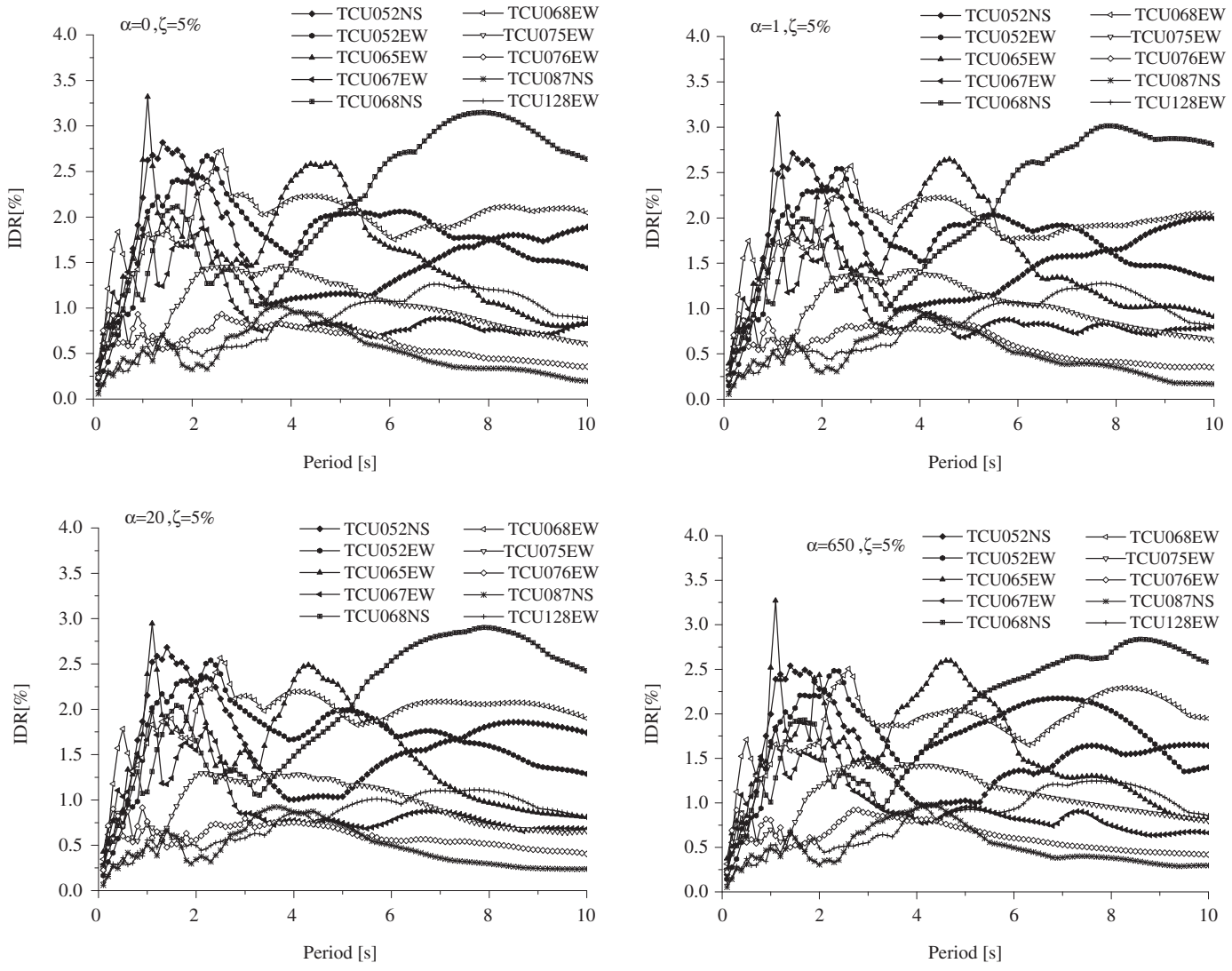


**Fig. 15.** Interstory drift spectrum of near-fault ground motions with fling-step pulses for $\alpha=0$, 1, 20 and 650.

pulses presents at the height $z/H=0.18$. Nevertheless, the largest mean $IDR=1.25\%$ under ground motions with fling-step pulses occurring at the height $z/H=0.15$ slightly lower than the former height. It again implies that the ground motions with fling-step pulses tend to generate the fundamental-mode response compared to ground motions with forward directivity pulses, which is harmful to structural seismic safety. Similar to Sections 4.3 and 5, the cause for this phenomenon can be revealed based on the distinct characteristic of impulsive ground motions and drift spectral analysis. Moreover, it is noted that for the long-period systems ($T=3.0$ s), the average IDRs under non-pulse ground motions are fairly smaller than those under impulsive ground motions and are distributed more uniformly along the total height. Therefore, the non-pulse ground motions lead to less damage potential for long-period structures.

## 7. Conclusions

Interstory drift ratios of building structures subjected to near-fault ground motions are examined systematically in this paper. The near-fault ground motions considered contain non-pulse motions and two kinds of impulsive ground motions with forward directivity and fling-step effects from Chi-Chi, Taiwan earthquake and Northridge, California earthquake. Meanwhile, three types of idealized simple pulses are applied to mimic the impulsive ground motions. Furthermore, the building systems are equivalently taken as flexural-shear cantilever beams with representative lateral stiffness ratios ($\alpha=0$, 1, 20 and 650), and the generalized interstory drift spectrum is introduced in terms of the wave propagation and modal superposition.

The general drift spectral analysis under simple pulses is implemented. The IDR demands under simple pulses provide some insight in distinguishing the dynamic responses of typical buildings to variations of pulse characteristics. It is shown that the simple pulses with forward directivity produce more intense drift demands, and the pulses having multiple cycles result in larger drift ratios due to the cumulative effects. Moreover, the fling-step pulses tend to excite primarily the first-mode response for moment-resisting frame building ($\alpha=20$), which agrees with the observation for the real buildings in the literature.

The IDR distributions of continuous beams subjected to three groups of near-fault ground motions are obtained. It is illustrated

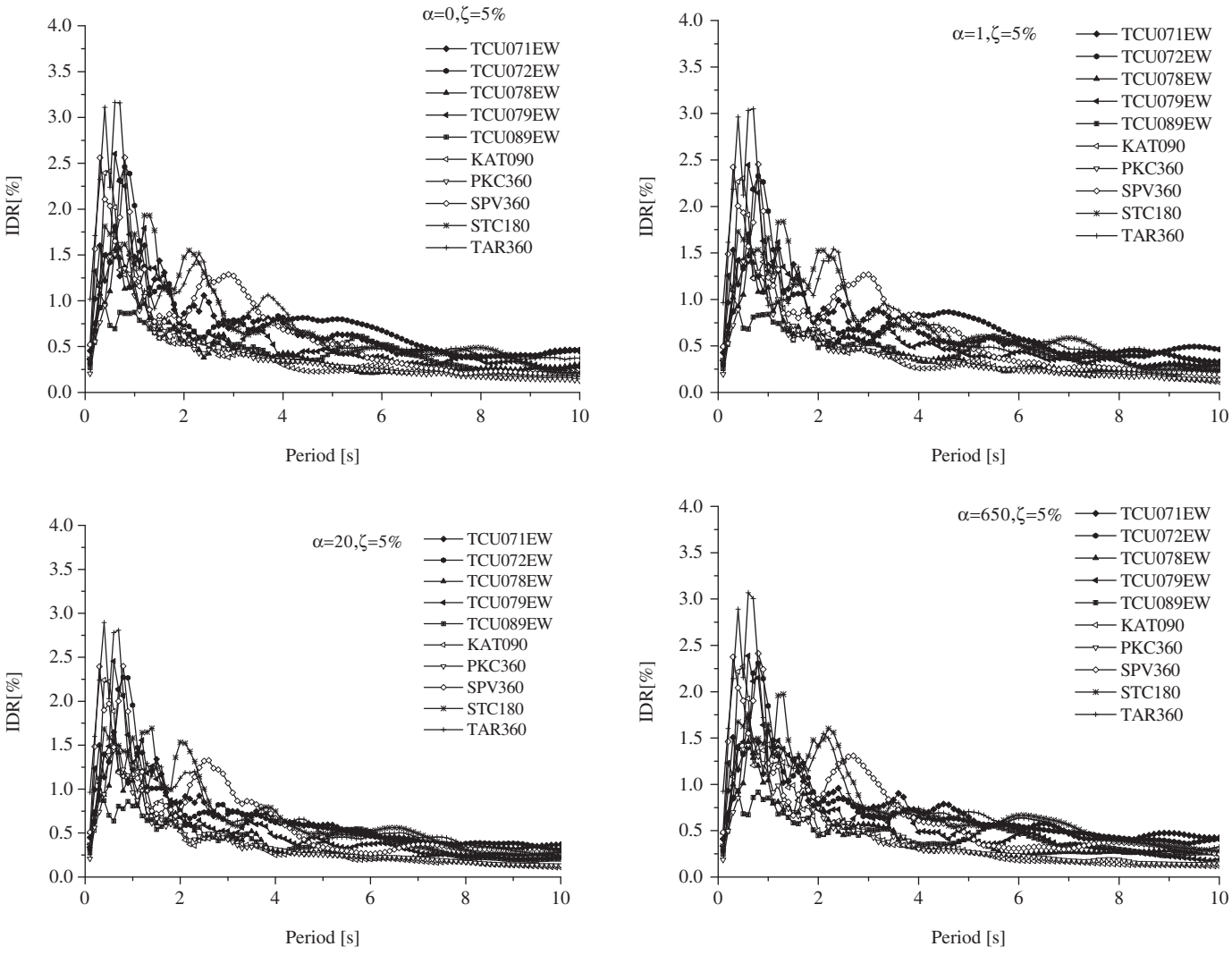


**Fig. 16.** Interstory drift spectrum of near-fault ground motions without pulse for $\alpha$=0, 1, 20 and 650.

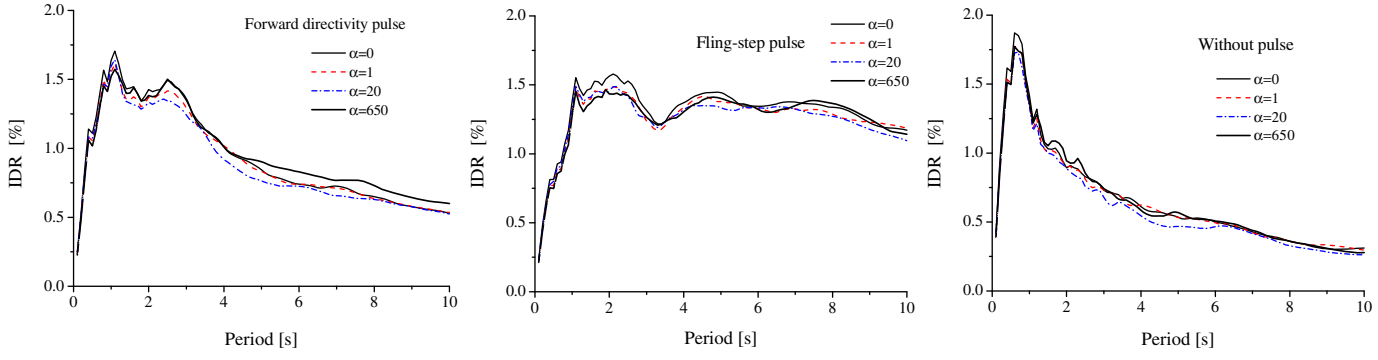


**Fig. 17.** Mean interstory drift spectrum of three groups of near-fault ground motions for $\alpha$=0, 1, 20 and 650.

that the maximum IDR shifts from the upper half to the lower half of buildings with increase in lateral stiffness ratio. For long-period systems ($T > 2.0$ s), the average IDR under impulsive ground motions is significantly greater than those under non-pulse ground motions. Finally, for moment-resisting frame buildings, the ground motions with forward directivity pulses activate the drift response of higher modes, while the ground motions with fling-step pulses excite primarily their contribution in the fundamental mode and lead to a large deformation in the lower stories, which is detrimental to structural safety. The essential cause for this phenomenon is exposed based on the distinct property of near-fault impulsive ground motions and drift spectral analysis.

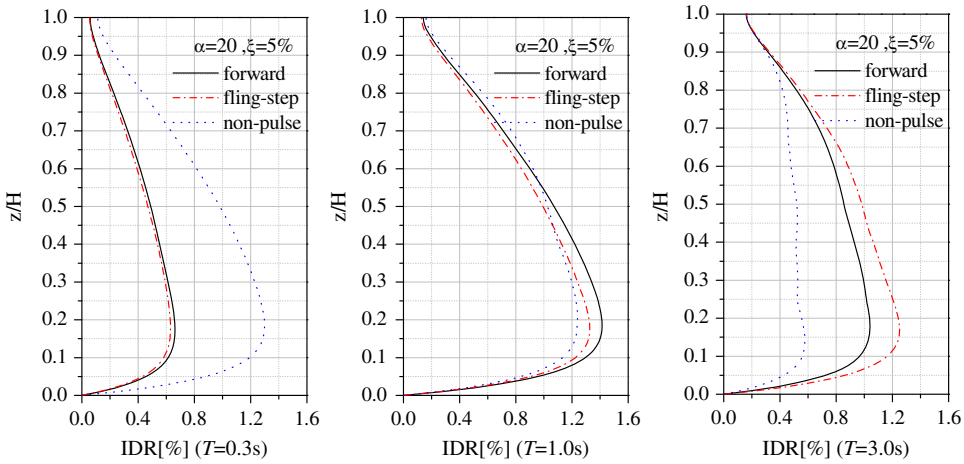


**Fig. 18.** Mean IDR distribution of buildings under three groups of near-fault ground motions with fundamental periods $T=0.3$, 1.0 and 3.0 s.

## Acknowledgments

The supports of the National Natural Science Foundation of China (Grant nos. 90815023 and 50978047) and the Key Project of Chinese National Programs for Fundamental Research and Development (Grant nos. 2006CB601205, 2010CB832703) are much appreciated. Also, we greatly appreciate one anonymous reviewer for his/her insightful suggestions and comments on the early version of this paper.

## References

[1] Iwan WD. Drift spectrum: measure of demand for earthquake ground motions. Journal of Structural Engineering 1997;123(4):397–404.
[2] Chopra AK, Chintanapakdee C. Drift spectrum versus modal analysis of structural response to near-fault ground motions. Earthquake Spectra 2001;17(2):221–34.
[3] Kim J, Collins KR. Closer look at the drift demand spectrum. Journal of Structural Engineering 2002;128(7):942–5.
[4] Gulkan P, Akkar S. A simple replacement for the drift spectrum. Engineering Structures 2002;24:1477–84.
[5] Huang CT. Considerations of multimode structural response for near-field earthquakes. Journal of Engineering Mechanics 2003;129(4):458–67.
[6] Roberts MW, Lutes LD. Potential for structural failure in the seismic near field. Journal of Engineering Mechanics 2003;129(8):927–34.
[7] Huang CT, Iwan WD. Generalized damped wave approach for evaluating seismic shear demands. Journal of Engineering Mechanics 2005;131(12):1248–56.
[8] Kim JK, Collins KR, Lim YM. Application of internally damped shear beam model to analysis of buildings under earthquake: Robust procedure for quick evaluation of seismic performance. Journal of Structural Engineering 2006;132(7):1139–49.
[9] Sasani M, Makris N, Bolt BA. Damping in shear beam structures and estimation of drift response. Journal of Engineering Mechanics 2006;132(8):851–8.
[10] Zembaty Z. Non-stationary random vibrations of a shear beam under high frequency seismic effects. Soil Dynamics and Earthquake Engineering 2007;27:1000–11.
[11] Miranda E, Akkar SD. Generalized interstory drift spectrum. Journal of Structural Engineering 2006;132(6):840–52.
[12] Somerville PG, Smith NF, Graves RW, Abrahamson NA. Modification of empirical strong ground motion attenuation relations to include the amplitude and duration effects of rupture directivity. Seismological Research Letters 1997;68(1):199–222.
[13] Somerville PG. Seismic hazard evaluation. In: Proceedings of 12th world congress on earthquake engineering, 2000, Paper: 2833, New Zealand.
[14] Wang GQ, Zhou XY, Zhang PZ, Igel H. Characteristics of amplitude and duration for near fault strong ground motion from the 1999 Chi-Chi, Taiwan, earthquake. Soil Dynamics and Earthquake Engineering 2002;22(1):73–96.
[15] Somerville PG. Magnitude scaling of the near fault rupture directivity pulse. Physics of the Earth and Planetary Interiors 2003;137:201–12.
[16] Bray JD, Rodriguez-Marek A. Characterization of forward-directivity ground motions in the near-fault region. Soil Dynamics and Earthquake Engineering 2004;24(5):815–28.
[17] Kalkan E, Kunnath SK. Effects of fling step and forward directivity on seismic response of buildings. Earthquake Spectra 2006;22(2):367–90.
[18] Anderson JC, Bertero VV. Uncertainties in establishing design earthquake. Journal of Structural Engineering 1987;113(8):1709–24.
[19] Hall JF, Heaton T H, Halling MW, Wald DJ. Near-source ground motion and its effects on flexible buildings. Earthquake Spectra 1995;11(4):569–605.
[20] Malhotra PK. Response of buildings to near-field pulse-like ground motions. Earthquake Engineering and Structural Dynamics 1999;28:1309–26.
[21] Makris N, Chang SP. Effects of viscous, viscoplastic and friction damping on the response of seismic isolated structures. Earthquake Engineering and Structural Dynamics 2000;29:85–107.
[22] Liao WI, Loh CH, Wan S. Earthquake response of RC moment frames subjected to near-fault ground motions. The Structural Design of Tall Buildings 2001;10:219–29.
[23] Mavroeidis GP, Papageorgiou AS. A mathematical representation of near-fault ground motions. Bulletin of the Seismological Society of America 2003;93(3):1099–131.
[24] Alavi B, Krawinkler H. Behavior of moment-resisting frame structures subjected to near-fault ground motions. Earthquake Engineering and Structural Dynamics 2004;33:687–760.
[25] Mavroeidis GP, Dong G, Papageorgiou AS. Near-fault ground motions, and the response of elastic and inelastic single-degree-of-freedom system. Earthquake Engineering and Structural Dynamics 2004;33:1023–49.
[26] Akkar S, Yazgan U, Gulkan P. Drift estimates in frame building subjected to near-fault ground motions. Journal of Structural Engineering 2005;131(7):1014–24.
[27] Tothong P, Cornell CA. Structural performance assessment under near-source pulse-like ground motion intensity measures. Earthquake Engineering and Structural Dynamics 2008;37(10):1013–37.
[28] Spyrakos CC, Maniatakis CA, Taflambas J. Evaluation of near-source seismic records based on damage potential parameters case-study. Greece. Soil Dynamics and Earthquake Engineering 2008;28:738–53.
[29] Yang DX, Pan JW, Li G. Non-structure-specific intensity measure parameters and characteristic period of near-fault ground motions. Earthquake Engineering and Structural Dynamics 2009;38(11):1257–80.
[30] Krawinkler H, Medina R, Alavi B. Seismic drift and ductility demands and their dependence on ground motions. Engineering Structures 2003;25:637–53.
[31] Alavi B, Krawinkler H. Strengthening of moment-resisting frame structures against near-fault ground motions effects. Earthquake Engineering and Structural Dynamics 2004;33:707–22.
[32] Miranda E, Reyes CJ. Approximate lateral drift demands in multistory buildings with nonuniform stiffness. Journal of Structural Engineering 2002;128(7):840–9.
[33] Cuesta I, Aschheim MA. The use of simple pulses to estimate inelastic response spectra. Journal of Earthquake Engineering 2004;8(6):865–93.